

Tunneling-assisted impact ionization fronts in semiconductors

P. Rodin*

*Institute for Theoretical Physics, Technical University Berlin, Hardenbergstrasse 36, 10623 Berlin, Germany
Centrum voor Wiskunde en Informatica, P.O.Box 94079, 1090 GB Amsterdam, The Netherlands*

U. Ebert and W. Hundsdorfer

Centrum voor Wiskunde en Informatica, P.O.Box 94079, 1090 GB Amsterdam, The Netherlands

I.V. Grekhov

*Ioffe Physicotechnical Institute, Politechnicheskaya 26, 194021, St. Petersburg, Russia
(November 3, 2018)*

We propose a novel type of ionization front in layered semiconductor structures. The propagation is due to the interplay of band-to-band tunneling and impact ionization. Our numerical simulations show that the front can be triggered when an extremely sharp voltage ramp (~ 10 kV/ns) is applied in reverse direction to a Si $p^+ - n - n^+$ -structure that is connected in series with an external load. The triggering occurs after a delay of 0.7 to 0.8 ns. The maximal electrical field at the front edge exceeds 10^6 V/cm. The front velocity v_f is 40 times faster than the saturated drift velocity v_s . The front passes through the n -base with a thickness of $100 \mu\text{m}$ within approximately 30 ps, filling it with dense electron-hole plasma. This passage is accompanied by a voltage drop from 8 kV to dozens of volts. In this way a voltage pulse with a ramp up to 500 kV/ns can be applied to the load. The possibility to form a kilovolt pulse with such a voltage rise rate sets new frontiers in pulse power electronics.

PACS numbers: 85.30.Mn, 72.20.Ht, 05.65.+b

I. INTRODUCTION

Impact ionization and tunneling (Zener breakdown) are the two most fundamental mechanisms capable of creating high concentrations of free carriers in a semiconductor within a short time interval. The respective threshold electrical fields differ by almost one order of magnitude, e.g., $2 \cdot 10^5$ V/cm and 10^6 V/cm for impact and tunneling ionization in Si, respectively^{1,2}. Avalanche impact ionization can be easily achieved by applying a sufficiently strong external electrical field. This process underlies the operation of many semiconductor devices such as avalanche transistors, IMPATT and TRAPATT diodes, *etc.*¹⁻³. The most interesting scenario corresponds to the propagation of a *superfast ionization front*: a narrow impact ionization region travels from the cathode to the anode with a velocity v_f much higher than the saturated drift velocity v_s , leaving a high density plasma behind⁴⁻⁹. In contrast to impact ionization, direct tunneling of electrons from the valence to the conductance band is hard to achieve in the bulk of uniformly doped semiconductor layers: while the applied external voltage is being increased, impact ionization typically sets in first, inducing an avalanche multiplication of free carriers. This causes the conductivity to increase and prevents further increase of the applied voltage. For this reason, tunneling ionization is generally assumed to be relevant only in heavily doped $p - n$ -junctions due to the strong internal electrical fields¹.

In this article we demonstrate that the threshold of tunneling ionization in the bulk of a Si $p^+ - n -$

n^+ -structure can be reached under the same experimental conditions as for triggering impact ionization fronts⁶⁻⁹. Typically a solitary ionization front is triggered by applying a sharp voltage ramp (≥ 1 kV/ns) to the $p^+ - n - n^+$ -structure in reverse direction^{6,9,10}. In structures with kilovolt $p - n$ -junctions and large cross-sections, this process is used for sharpening electrical pulses^{9,11-13}. This technique allows one to reach voltage ramps of up to 10 kV/ns, the state of the art in modern pulse power electronics. We demonstrate, that when such a sharp ramp $A \sim 10$ kV/ns is applied to a fully depleted reversely biased Si $p^+ - n - n^+$ -structure, the threshold of tunneling ionization $\sim 10^6$ V/cm is reached after less than 1 ns, which turns out to be faster than the initiation of avalanche impact ionization. The resulting breakdown takes the form of an ionization front that propagates due to the combined effect of tunneling and impact ionization. Compared to the traditional impact ionization fronts in pulse sharpening diodes^{6-9,11,12} and TRAPATT-diodes^{4,5}, these *tunneling-assisted impact ionization fronts* are expected to be much faster and generate higher plasma concentrations. Their practical application may set new frontiers in pulse power electronics.

II. THE MODEL

We consider a Si $p^+ - n - n^+$ -structure with sharp $p^+ - n$ and $n - n^+$ -transitions and the following parameters: the width of the n -base is $W = 100 \mu\text{m}$, the cross-

section area is $S = 0.002 \text{ cm}^2$, the doping levels are $N_d \approx 10^{14} \text{ cm}^{-3}$ in the n -base and $N_{a,d}^+ \approx 10^{19} - 10^{20} \text{ cm}^{-3}$ in the contact p^+ - and n^+ -layers, respectively. These parameters correspond to a typical Si power diode with a stationary breakdown voltage $\sim 1.5 \text{ kV}^1$. We choose the initial bias of $V_0 = 1 \text{ kV}$, closely below the voltage of stationary avalanche breakdown. For this bias, the n -base is fully depleted from major carriers (electrons) and equilibrium minor carriers (holes).

The device is connected to a voltage source $V(t)$ in series with a load resistance $R = 50 \Omega$ as sketched in Fig. 1. Since it is convenient to work with a positive electrical field E for the reverse bias, we put the $n - n^+$ -junction on the l.h.s. at $z = 0$ and the $p^+ - n$ -junction on the r.h.s. at $z = W$. The voltage $V(t)$ applied to the structure and the load is in linear approximation

$$V(t) = V_0 + At, \quad (1)$$

where A is the voltage ramp. Hereinafter we keep $A = 10 \text{ kV/ns}$. The voltage on the device is denoted as $U(t)$ and related to $V(t)$ through the Kirchhoff equation $V = U + RI$, where I is the total current.

We use a minimal model which accounts only for the basic transport processes, for band-to-band impact ionization and tunneling ionization. The continuity equations for electrons and holes n and p are written in one-dimensional approximation

$$\partial_t n - \partial_z (v_n(|E|) n) = G(n, p, |E|), \quad (2)$$

$$\partial_t p + \partial_z (v_p(|E|) p) = G(n, p, |E|). \quad (3)$$

and complemented by the Poisson equation

$$\partial_z E = \frac{q}{\varepsilon \varepsilon_0} (p - n + N_d(z) - N_a(z)) \quad (4)$$

and the Kirchhoff equation. We assume drift-dominated transport and approximate the carrier velocities as¹⁴

$$v_n(|E|) = v_s \frac{|E|}{E_{sn} + |E|}, \quad v_p(|E|) = v_s \frac{|E|}{E_{sp} + |E|}, \quad (5)$$

$$\text{where} \quad v_s = 10^7 \text{ cm/s}, \quad (6)$$

$$E_{sn} = 8.0 \cdot 10^3 \text{ V/cm}, \quad E_{sp} = 2.32 \cdot 10^4 \text{ V/cm}.$$

Since the ionization processes are fast and develop in the bulk of the device, we solve these equations in the n -base only. The different effect of $p^+ - n$ - and $n - n^+$ -junctions on electron and hole concentrations in the n -base is modelled by mixed boundary conditions: $\partial_z n = 0$, $p = 0$ at $z = 0$ and $\partial_z p = 0$, $n = 0$ at $z = W$ ¹⁵. The generation term $G(n, p, |E|)$ contains band-to-band tunneling and impact ionization terms:

$$G(n, p, |E|) = G_T(|E|) + G_I(n, p, |E|), \quad (7)$$

The tunneling term $G_T(|E|)$ models electron tunneling from the valence band to the conduction band¹⁶

$$G_T(|E|) = \alpha_T E^2 e^{-b_T/|E|}, \quad (8)$$

$$\alpha_T = \frac{q^2}{3\pi^2 \hbar^2} \sqrt{\frac{2m}{E_g}}, \quad b_T = \frac{\pi}{4q\hbar} \sqrt{2mE_g^3},$$

where q and m are electron charge and effective mass, respectively, E_g is the bandgap, and \hbar is Planck's constant. The impact ionization term $G_I(n, p, |E|)$ is chosen as

$$G_I(n, p, |E|) = \alpha_n(|E|) v_n(|E|) n \Theta(n - n_{cut}) + \alpha_p(|E|) v_p(|E|) p \Theta(p - p_{cut}), \quad (9)$$

$$\alpha_n(|E|) \equiv \alpha_{ns} e^{-b_n/|E|}, \quad \alpha_p(|E|) \equiv \alpha_{ps} e^{-b_p/|E|}, \quad (10)$$

where the impact ionization coefficients and the characteristic fields are given by¹⁷

$$\alpha_{ns} = 7.4 \cdot 10^5 \text{ cm}^{-1}, \quad \alpha_{ps} = 7.25 \cdot 10^5 \text{ cm}^{-1},$$

$$b_n = 1.1 \cdot 10^6 \text{ V/cm}, \quad b_p = 2.2 \cdot 10^6 \text{ V/cm}, \quad (11)$$

and $\Theta(x)$ is the step-function. The cut-offs n_{cut} and p_{cut} have been introduced in (9) to mimic the discreteness of the charge carriers. The purpose is to exclude unphysical ionization avalanches initiated by tiny fractions of electrons or holes that can cause premature triggering of the front in the simulations. We chose $n_{cut} = p_{cut} = 10^9 \text{ cm}^{-3}$ in the simulations and discuss the effect of this and other choices in Section V and Fig. 6.

Since we shall investigate processes on a sub-nanosecond time scale, we neglect all types of recombination and thermal generation. We also assume that the n -base is free of deep-level defects or parasitic impurities that can assist tunneling or serve as deep-level electron traps capable to release electrons or holes in high electric field¹⁸. We discuss these model assumptions in detail in Sections IV and V.

We use a uniform space-time grid with the number of points of the order of several thousands both in time and space. The spatial discretization is based on a conservative formulation, in terms of fluxes describing the inflow and outflow over cells $[x - \Delta x/2, x + \Delta x/2]$, where Δx is the grid width in space. Whereas the diffusive fluxes have been approximated in a standard fashion¹⁹ with second order accuracy, for the convective fluxes a third order upwind biased formula has been chosen in order to reduce the numerical oscillations. Time discretization is based on a second order backward differentiation formula. The temporal backward differentiation formula gives an implicit system that is solved at each time step. For reasons of accuracy the time step Δt is chosen small compared to $\Delta x/v_s$, where v_s is the upper bound of the drift (convective) velocity, and with such small step size that the implicit system can be solved by a straightforward functional iteration. Details on these spatial and temporal discretizations can be found in Ref. 20.

III. NUMERICAL SOLUTIONS

The basic features of the numerical solutions are summarized in Figures 2 and 3. They show the external characteristics of the transient and the internal dynamics, respectively. The voltage on the device first increases and reaches the maximal value 8 kV, several times higher than the voltage of stationary breakdown. During this stage, the electrical field in the structure increases like

$$E(x, t) \approx \frac{V(t)}{W} - \frac{bW}{2} + bx, \quad b \equiv \frac{qN_d}{\varepsilon\varepsilon_0}, \quad (12)$$

in the same manner as in the TRAPPAT-diode^{1,5}. (Here we assume that the displacement current is small and hence $V(t) \approx U(t)$). Though the electrical field E at the right boundary exceeds the effective threshold of impact ionization $2 \cdot 10^5$ V/cm already at $t > 30$ ps, impact ionization does not develop due to the absence of initial carriers. At $t \approx 720$ ps the electrical field at the right boundary $x = W$, near the $p^+ - n$ -junction, becomes sufficient for tunneling of electrons from the valence to the conduction band (Fig. 3(a), curve 1). At this time, the field is above the threshold of impact ionization in the whole n -base, so impact ionization starts as soon as electrons and holes are supplied by tunneling. The rate of impact ionization increases with concentration and eventually overcomes tunneling at the carrier density $n \sim p \sim 10^{13}$ cm⁻³ (see Fig. 4). The rapid ionization process near the right boundary forms an initial nucleus of dense electron-plasma with concentration $n, p \sim 2 \cdot 10^{17}$ cm⁻³ that is capable to fully screen the electrical field (Fig. 3(a), curves 2, 3). The screening is accomplished at $t = 750$ ps. It is accompanied by a fast drop of the voltage on the device and an increase of current in the circuit (Fig. 2). This drop corresponds to the first step in the falling $U(t)$ -curve.

Consecutively, the highly conducting plasma region expands to the left in the form of a superfast ionization front (Fig. 3(b)). The velocity of the front v_f is approximately 40 times faster than the saturated drift velocity v_s of the individual carriers; hence the carrier motion is negligible. The front propagates due to the combined effect of tunneling and impact ionization, followed by Maxwell relaxation in the generated plasma and consecutive electric screening. Snapshots of the field and concentration profiles together with respective generation rates at some instant of time are shown in Fig. 5. Here tunneling generates initial carriers in the high field region at the edge of the ionization front. These carriers are multiplied further by impact ionization. A narrow region of strong impact ionization is localized at the edge of the visible concentration front. The rate of impact ionization in this region is by many orders of magnitude higher than the rate of tunneling ionization. Therefore impact ionization dominates the overall increase of the concentration. However, the superfast propagation would not be possible without the initial carriers generated by tunneling. Hence

both tunneling and impact ionization are essential for the propagation mechanism. This type of an ionization front can be called a *tunneling-assisted impact ionization front*.

As the front propagates, the current I increases and the voltage on the device U decreases due to the interaction with the external load. The maximum value of the electrical field and the front velocity slightly increase during the passage (Fig. 3(b)). As the front comes closer to the left boundary, the field in the high-field region of the n -base increases and the region of tunneling impact ionization becomes wider. This effect also contributes to the acceleration of the front, and causes the front interface to become smoother (compare curves 1,2 and 3,4 in Fig. 3). Eventually, the tunneling process becomes efficient in the whole region between the moving front and the n^+ -contact. As a result, the front ceases to propagate. Rather the rest of the n -base breaks down by nearly uniform impact ionization.

The switching takes 30 ps and fills the n -base with electron-hole plasma of concentration $\sim 5 \cdot 10^{17}$ cm⁻³. The voltage drops from 8 kV to the residual value of 10 V, applying an average voltage ramp ~ 300 kV/ns to the load. The falling part of the $U(t)$ -dependence in Fig. 2 has a plateau that reflects the transition from the formation of the initial nucleus of electron-hole plasma to the stage of front propagation. During the front propagation stage, the voltage drops from ~ 7.4 kV to 10 V within less than 15 ps. Hence the "effective" voltage ramp is much higher than the average one and reaches 500 kV/ns.

IV. THE EFFECT OF RANDOM THERMAL GENERATION

The triggering of the tunneling-assisted impact ionization front might fail due to the thermal generation of free carriers in the depleted layer. If during an early stage of development, thermal carriers lead to an avalanche breakdown and to the formation of local conducting channels between the p^+ - and n^+ -layers, the conductance might increase and prevent the voltage $U(t)$ from increasing further. In this case, a front cannot start. Therefore the related time scales and their temperature dependence have to be estimated.

The characteristic rate of thermal generation of electron-hole pairs can be deduced from the value of the leakage current density. It is $\approx 10^{-7}$ A/cm² at room temperature^{6,9}. Hence on average, one thermal electron-hole pair per ns is generated in the whole volume of the n -base. Depending on the position of the generation, the carriers need 0.5 to 1 ns to leave the n -base of length 100 μ m with saturated drift velocity 10^7 cm/s. If the field is still low, they will simply leave the base, but if they are generated in a region with $E > 2 \cdot 10^5$ V/cm or pass

through such a region, they will create an impact ionization avalanche on their path. After 0.7 ns, the tunneling-assisted impact ionization front leads to the breakdown of the voltage. Though the probability that one ionization avalanche will be initiated during the delay time is close to one, this avalanche in most cases cannot form a conducting channel before the front is triggered. The probability for more avalanches decreases exponentially with their number.

However, even if a single conducting channel has developed, its cross-section is too small compared to the cross-section of the system to influence the triggering of the superfast front. Typical diameters of local conducting channels created by solitary avalanches are about $10\text{ }\mu\text{m}$ ²¹, so the cross-section is about 1/1000 of the total cross-section of the semiconductor structure. Assuming concentrations of $n, p \sim 10^{18}\text{ cm}^{-3}$ and high-field transport with saturated velocities v_s , we evaluate the maximum current that can flow through such channel as $\sim 1\text{ A}$ ²². This is comparable to the displacement current in the structure during the delay stage, and far too small to prevent the further increase of the voltage on a structure with large cross-section.

The generation rate depends exponentially on the temperature¹:

$$\nu(T) = \nu(T_0) \exp\left(\frac{E_g}{kT_0} - \frac{E_g}{kT}\right), \quad (13)$$

where k is Boltzmann's constant and T_0 is room temperature. For $T = 70\text{ K}$ and $T = 400\text{ K}$, we find characteristic times of $\tau \sim 10\text{ ms}$ and $\tau \sim 1\text{ ps}$, respectively. Hence the triggering mechanism is very sensitive to the temperature of the structure: cooling the sample is favorable whereas triggering of tunneling-assisted fronts is likely to be impossible at high temperatures.

We conclude that the tunneling-assisted impact ionization front can be triggered only, if the applied voltage increases sufficiently fast and the threshold of tunneling ionization is reached faster than 1 ns. At room temperature and below, the triggering mechanism is robust with respect to random initiation of impact ionization avalanches by thermal carriers. This conclusion is also supported by experimental data for common impact ionization fronts^{6,9}: for comparable experimental set-up and the lower voltage ramp of $A \sim 1\text{ kV/ns}$, the delay in deterministic triggering of the impact ionization front could be as large as 3 ns.

V. LIMITATIONS OF THE DRIFT-DIFFUSION MODEL

In this section, we discuss the applicability of the minimal drift-diffusion model to the rapid high-field process described in Sec. III. Let us first briefly summarize the characteristic scales of the obtained numerical solution: the front length is $\ell_f \sim 3\text{ }\mu\text{m}$, the front velocity

$v_f \sim 4 \cdot 10^8\text{ cm/s}$, the total switching time $\sim 30\text{ ps}$, the concentration behind the front $\sim 5 \cdot 10^{17}\text{ cm}^{-3}$, and the current density $J \sim 10^5\text{ A/cm}^2$.

Relaxation time and electro-magnetic propagation time. A simple evaluation in the spirit of Drude theory and based on the low-field mobility, estimates the upper bound for the electron mean free path and the lower bound for the electron momentum relaxation time as 20 nm and 0.2 ps, respectively. The electro-magnetic propagation time is $W/c = 0.5\text{ ps}$, where c is the speed of light. These scales are considerably smaller than the respective scales of the process under study.

Recombination. In Si for concentrations $n = p = 10^{18}\text{ cm}^{-3}$, the inverse rate of Auger recombination is $\sim 10\text{ }\mu\text{s}$; the thermal recombination life-time is also of the order of microseconds²³. Thus recombination can be neglected.

Electron-hole scattering. For current densities above 10^2 A/cm^2 , electron-hole scattering which is not accounted for in our model, becomes important²⁴. Due to the electron-hole scattering, the resistivity ρ of the dense plasma behind the front substantially decreases. For $J \sim 10^3\text{ A/cm}^2$ and $n, p \sim 10^{18}\text{ cm}^{-3}$ we estimate the order of the magnitude as $\rho \sim 1\text{ }\Omega \cdot \text{cm}$ ²⁴. Hence the voltage drop across the n -base after switching can be estimated as $J\rho W \sim 10\text{ V}$. This value should be added to the 10 V obtained in our simulations. (Note that in our model the residual voltage is mostly due to the recovery of the electrical field on the $p^+ - n$ -junction during the front propagation.) This difference of 10 V is negligible compared to the kilovolt voltage drop during the front passage, and does not change other characteristics of the switching process.

Continuum approximation. The continuum treatment of electron and hole concentrations is the major limitation of the standard drift-diffusion model in application to the present problem. Both tunneling and impact ionization terms ignore the discrete nature of the ionization process: The tunneling term predicts a small but steady increase of the concentration even for electrical fields that are far below the effective threshold of tunneling ionization. In turn, the impact ionization generation term (10) models the multiplication of any concentration of free carriers, even if these concentrations physically correspond to a tiny fraction of an electron or hole in the whole volume of the device. Since, first, these small concentrations of initial carriers are inherently present in the system at the early stages of the process and, second, the system is very sensitive to the appearance of free carriers in the high field region, the unreflected use of an continuum approximation leads to physically meaningless results: triggering of the front is observed at very low electrical fields due to the multiplication of unphysically small concentrations of free carriers. Such an unphysical solution that predicts premature triggering of the front is depicted by the dashed line in Fig. 6: the front is triggered at $t \approx 300\text{ ps}$ when the maximum electrical field is

not more than $E(W, t) = 5 \cdot 10^5$ V/cm, which is too low for tunneling ionization.

These unphysical solutions can be eliminated by introducing the cut-offs for low concentrations in the impact ionization generation term (9). The cut-off concentrations n_{cut} and p_{cut} approximate the range of validity of the continuum approximation. Carefully chosen cut-offs allow to avoid the artifacts and to provide qualitatively relevant results. In Fig. 6, we show the transient characteristics for different cut-offs n_{cut} . In a wide range of physically meaningful parameter values of n_{cut} , the front triggering and propagation is qualitatively the same. However, the time delay in the front triggering somewhat depends on the cut-off level, thus making the continuum model unsuitable for accurate quantitative predictions. The delay time shifts by approximately 50 ps when the cut-off level changes by one order of magnitude in both directions, whereas the triggering time remains approximately the same. A quantitative analysis would demand a more elaborate stochastic microscopic model.

VI. DISCUSSION

Tunneling-assisted impact ionization fronts are quite similar to the well studied case of superfast impact ionization fronts that underly the operation of TRAPPAT-diodes^{4,5} and sharpening diodes^{6,7,9,11,12}. In both cases we deal with a collective phenomenon of superfast propagation. It is based on avalanche multiplication of the already existing carriers due to impact ionization in a finite narrow region of the device, followed by screening of the electrical field due to Maxwell relaxation in the adjacent spatial region. The important difference is the source of the free carriers that initiate the avalanche impact ionization process. TRAPPAT-like fronts propagate into a depleted n -base with a certain concentration of initial carriers, often referred to as "pre-ionization"^{25,26}. The physical mechanism that creates "pre-ionization" then is unrelated to the front propagation mechanism, e.g., in the case of the TRAPPAT-diode, these are non-equilibrium carriers left behind after the previous front passage. In the case under consideration here, there is no pre-ionization and the initial carriers are generated during the front passage by tunneling in a region just ahead of the impact ionization front. Hence tunneling and impact ionization coherently cooperate in the superfast propagation of the tunneling-assisted impact ionization front.

For impact ionization fronts that propagate into homogeneously pre-ionized media, an essential ingredient is the spatial profile of the electrical field: the field should be below the threshold of impact ionization at a certain distance from the front^{5,25,26}. This keeps the "active" region where the impact ionization develops, finite and prevents a quasi-uniform blow-up of the concentration in the whole

sample. For ionization fronts in $p^+ - n - n^+$ -structures this profile is due to the doping of the n -base that gives a slope of the electrical field $qN_d/\epsilon\epsilon_0$ in the depleted layer. In contrast, for the tunneling-assisted front, the electrical field is well above the threshold of impact ionization in the whole n -base. The size of the "active" region is controlled by the threshold of tunneling ionization. This allows for much higher electrical fields, increasing the front velocity and the concentration of the generated plasma by orders of magnitude.

The possibility of tunneling ionization fronts has been discussed before in Ref. 27. The theoretical investigation in Ref. 27 takes only tunneling ionization into account, assuming that in high fields the impact ionization component can be neglected. Our results show that this is not possible for electrical fields of the order of 10^6 V/cm: the importance of impact ionization increases with concentration and dominates tunneling ionization already for concentrations of free carriers as low as $n, p > 10^{13}$ cm⁻³, as can be read from Fig. 4. Thus impact ionization is the dominant mechanism of free carrier generation even in the range of fields where tunneling is possible, after a sufficient carrier concentration is reached. Accordingly, simulations with the impact ionization term set to zero show that the tunneling ionization alone does not lead to front propagation; rather the breakdown of the sample becomes quasi-uniform. We suggest the following explanation for this observation: the appearance of the traveling front solutions is known to be due to an auto-catalytic dependence of the impact ionization generation rate on the concentration of initial carriers^{5,25,26,28}. It leads to the exponentially fast increase of the concentration with time in a given electrical field. The rate of tunneling ionization lacks this auto-catalytic dependence on the concentration, predicting an algebraically slow growth of concentration with time.

VII. SUMMARY

We have described the theory of a new type of ionization fronts in layered Si semiconductor structures. These are superfast tunneling-assisted impact ionization fronts that propagate due to the coherent effect of tunneling and impact ionization. The front propagates into the fully depleted n -base of a $p^+ - n - n^+$ -structure. The region of tunneling ionization in electrical fields higher than 10^6 V/cm has a characteristic length of dozens of micrometers. The generated carriers initiate an avalanche impact ionization process that becomes much more efficient than tunneling as concentration increases. The concentration front has a characteristic width of several micrometers. Within this length the concentration of free carriers increases to the level of $n, p > 5 \cdot 10^{17}$ cm⁻³. Maxwell relaxation in the generated electron-hole plasma leads to the full screening of the applied electrical field. The front propagation is a collective phenomenon based

on ionization and screening, and its velocity v_f is not limited by the high-field drift velocity of individual carriers v_s . We observe $v_f \approx 40 \cdot v_s$ in our simulations.

The front triggering becomes possible if the threshold of tunneling ionization 10^6 V/cm is reached after a delay shorter than 1 ns. This ensures that random thermal ionization in the depleted layer does not spoil the triggering. This condition is met at room and lower temperatures when a voltage ramp ~ 10 kV/ns is applied to the structure connected in series with a load. Such voltage pulses are state of the art in modern semiconductor pulse power electronics⁹. The passage of the tunneling-assisted impact ionization front switches the structure into the conducting state with a residual voltage of several dozens of volts. The transient $U(t)$ –characteristic is nonlinear: the total duration of the switching process observed is 30 ps, whereas the effective switching time that corresponds to the major voltage drop is below 15 ps. Hence a voltage pulse of rise rate ~ 500 kV/ns and an amplitude of several kilovolts is applied to the load. These values set new frontiers in pulse power electronics.

We finally remark, that the standard drift-diffusion model has serious limitations when applied to models of superfast ionization fronts. These limitations are due to the continuum approximation. They manifest themselves in a premature unphysical triggering of the front at low electrical fields due to avalanche processes initiated by tiny fractions of electrons or holes. We have eliminated these unphysical solutions by introducing a cut-off in the impact ionization term. For further progress towards a fully quantitative description, microscopic stochastic model have to be investigated.

ACKNOWLEDGMENTS

This work was supported by the Dutch physics funding agency FOM and the program “Generation of high power pulses of electrical energy, particles and electro-magnetic radiation” of the Presidium of the Russian Academy of Sciences. P.R. also acknowledges support of the Alexander von Humboldt Foundation.

* On leave from Ioffe Physicotechnical Institute, Politechnicheskaya 24, 194021, St. Petersburg, Russia.

¹ S. M. Sze, *Physics of Semiconductor Devices* (Wiley, New York, 1981).

² M. Shur, *Physics of Semiconductor Devices* (Prentice-Hall, Englewood Cliffs, 1990).

³ M. Shaw, V. Mitin, E. Schöll and H. Grubin, *The Physics on Instabilities in Solid State Electron Devices* (Plenum Press, New York, 1992).

- ⁴ H. J. Prager, K. K. N. Chang and J. Wiesbord, *Proc. IEEE* **55**, 586 (1968).
- ⁵ B. C. Deloach and D. L. Scharfetter, *IEEE Transactions Electron Devices* **ED-20**, 9 (1970).
- ⁶ I. V. Grekhov and A. F. Kardo-Sysoev, *Sov. Tech. Phys. Lett.* **5**, 395 (1979) [*Pis'ma Zh. Tekn. Fiz.* **5**, 950 (1979)].
- ⁷ D. Benz, M. Pocha, *Rev. Sci. Instr.* **56** 1456 (1985).
- ⁸ Zh. I. Alferov, I. V. Grekhov, V. M. Efanov, A. F. Kardo-Sysoev, V. I. Korol'kov, and M. N. Stepanova, *Sov. Tech. Phys. Lett.* **13**, 454 (1987) [*Pis'ma Zh. Tekn. Fiz.* **13**, 1089 (1987)].
- ⁹ I. V. Grekhov, *Sov. St. Electron.* **32**, 923 (1989).
- ¹⁰ A. Minarsky and P. Rodin, *Semiconductors* **34**, 665-667 (2000).
- ¹¹ R. J. Focia, E. Schamiloglu, C. B. Fledermann, F. J. Agee, J. Gaudet, *IEEE Transaction on Plasma Science*, **25**, 138 (1997).
- ¹² A. F. Kardo-Susoev, V. M. Efanov and I. G. Chashnikov, *Fast power switches from picosecond to nanosecond time scale and their application to pulsed power*, pp.342-347, in: *Dig. Techn. Papers, 10th IEEE Int. Pulsed Power Conf.*, edited by W. L. Baker and G. Cooperstain, Albuquerque, 1995.
- ¹³ V. A. Kozlov, A. F. Kardo-Susoev and V. I. Brulevsky, *Semiconductors* **35**, 608 (2001) [*Fiz. i Techn. Poluprov.* **35**, 629 (2001)].
- ¹⁴ C. Jacobini, C. Canali, G. Ottaviani and A. Alberigi, *Sol. Stat. Electron.* **20**, 77 (1977).
- ¹⁵ Our results are not sensitive to boundary conditions. In particular, the main characteristics of the process remains the same, if homogeneous Neumann boundary conditions are used for both electron and hole concentrations at both contacts.
- ¹⁶ E. Burstein and S. Lundqvist (eds.), *Tunneling phenomena in solids* (Plenum Press, New York, 1969).
- ¹⁷ V. A. Kuz'min, N. N. Krukova, A. S. Kuregyan, T. T. Mnatsakanov and V. B. Shuman, *Sov. Phys. Semicond.* **9**, 481 (1975) [*Fiz. Tekh. Poluprovodn.* **9**, 735 (1975)].
- ¹⁸ P. Rodin, U. Ebert, W. Hundsdorfer, and I. Grekhov, *Superfast fronts of impact ionization in initially unbiased layered semiconductor structures*, Report MAS-R0110, CWI, Amsterdam, <http://www.cwi.nl/static/publications/reports/abs/MAS-R0110.html>.
- ¹⁹ J. C. Strikwerda, *Finite difference schemes and partial differential equations*, (Chapman & Hall, New York, 1989).
- ²⁰ J. G. Verwer, W. Hundsdorfer, J. G. Blom, *Numerical time integration for air pollution models*, *Surveys on Mathematics for Industry*, Vol. 10/4 (2001), also available on <http://www.cwi.nl/static/publications/reports/abs/MAS-R9825.html>.
- ²¹ I. V. Grekhov and Yu. N. Serezkin, *Avalanche Breakdown of p-n-junctions in Semiconductors*, Energiya, Leningrad, 1980 (in Russian).
- ²² A. Minarsky and P. Rodin, *Sov. State Electron.* **31**, 366 (1997).
- ²³ P. T. Landsberg, *Recombination in semiconductors* (Cambridge University Press, Cambridge, 1991).
- ²⁴ T. I. Mnatsakanov, I. L. Rostovtzev and N. I. Philatov, *Solid State Electronics* **30**, 579 (1987).
- ²⁵ M. I. D'yakonov and V. Yu. Kachorovskii, *Sov. Phys. JETP*

67, 1049 (1988) [Zh. Eksp. Teor. Fiz. **94**, 321 (1988)].

²⁶ M. I. D'yakonov and V. Yu. Kachorovskii, Sov. Phys. JETP **68**, 1070 (1989) [Zh. Eksp. Teor. Fiz. **95**, 1850 (1989)].

²⁷ O.V. Konstantinov, O. A. Mezrin, Sov. Tech. Phys. Lett.

13, 197 (1987) [Pis'ma Zh. Tekn. Fiz. **13**, 476-481 (1987)].

²⁸ U. Ebert, W. van Saarloos and C. Caroli, Phys. Rev. Lett. **77**, 4178 (1996), Phys. Rev. E. **55**, 1530 (1997).

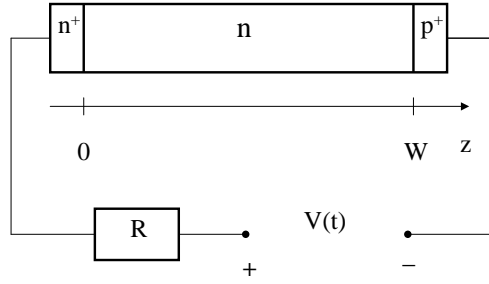


FIG. 1. Sketch of the $p^+ - n - n^+$ -structure operated in an external circuit with load resistance R .

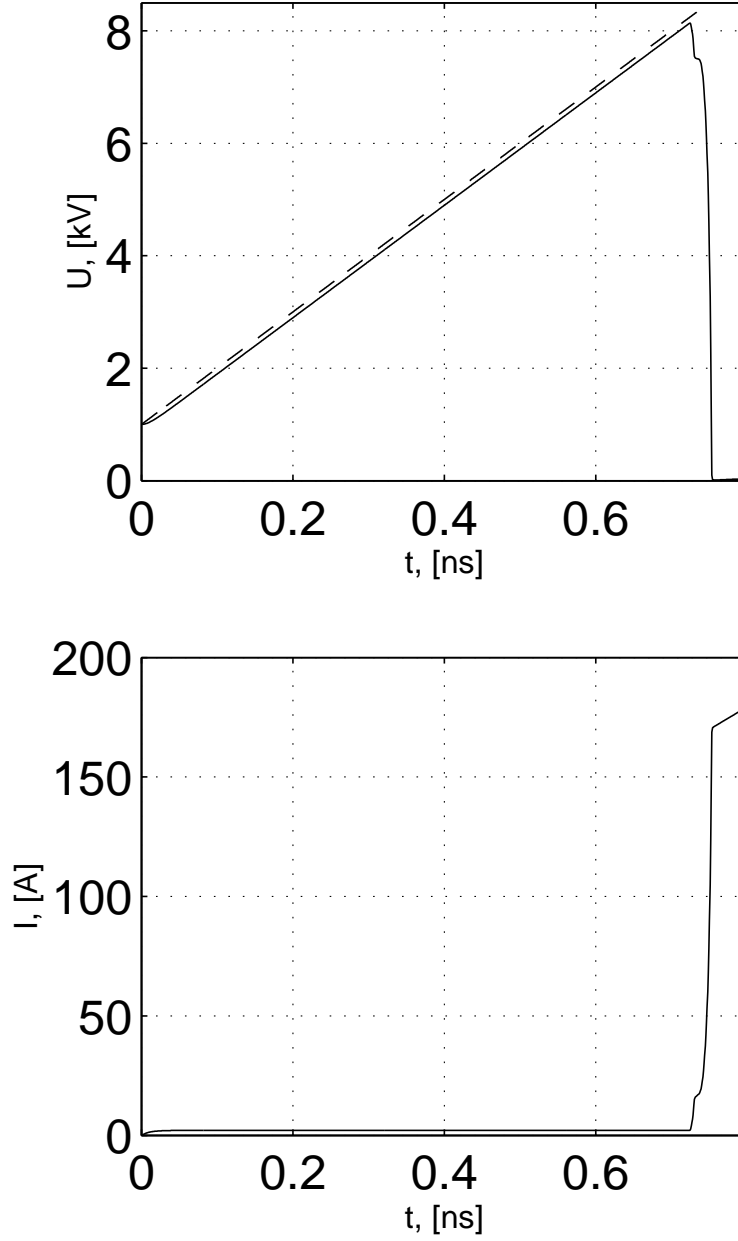


FIG. 2. Voltage at the structure $U(t)$ (solid line in the upper panel) and total current $I(t) = S J(t)$ (in the lower panel) during the switching process. The dashed line in the upper panel denotes the externally applied voltage $V(t)$. The quantities shown are related through Ohm's law $V = U + RI$. Parameters: $W = 100 \mu\text{m}$, $S = 0.002 \text{ cm}^2$, $N_d = 10^{14} \text{ cm}^{-3}$, $N_a = 0$, $V_0 = 1 \text{ kV}$, $A = 10 \text{ kV/ns}$, $R = 50 \Omega$, $n_{cut} = p_{cut} = 10^9 \text{ cm}^{-3}$.

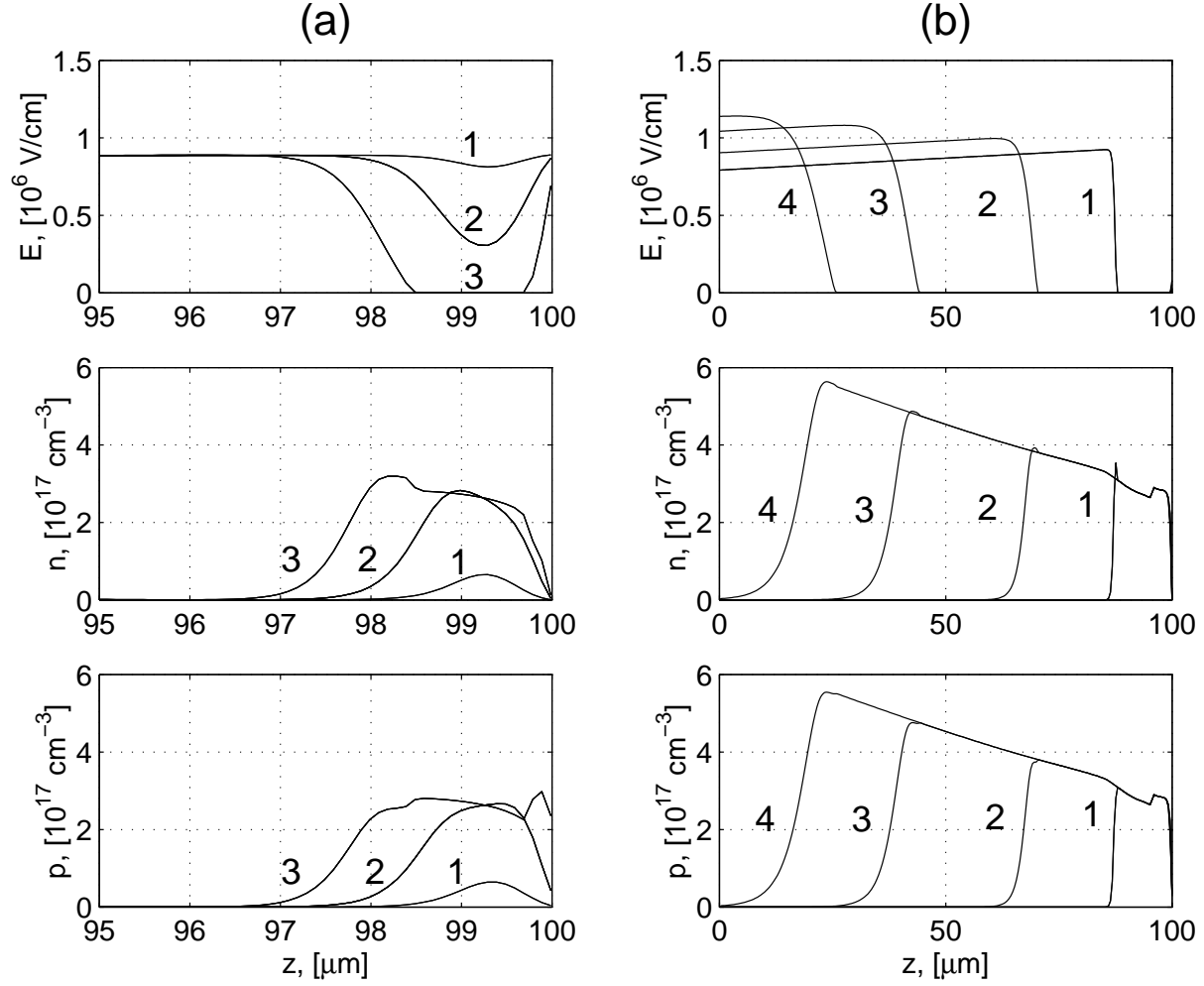


FIG. 3. The internal dynamics leading to the external characteristics of Fig. 2. Shown are the spatial profiles of the electrical field $E(x, t)$ and electron and hole concentrations $n(x, t)$, $p(x, t)$ in the n -base ($0 \leq z \leq W = 100 \mu\text{m}$) at different times: (a) nucleation of electron-hole plasma and triggering of the impact ionization front at times $t = 725, 726, 727$ ps (curves 1, 2, 3); (b) propagation of the tunneling-assisted ionization front at $t = 735, 745, 750, 752$ ps (curves 1, 2, 3, 4).

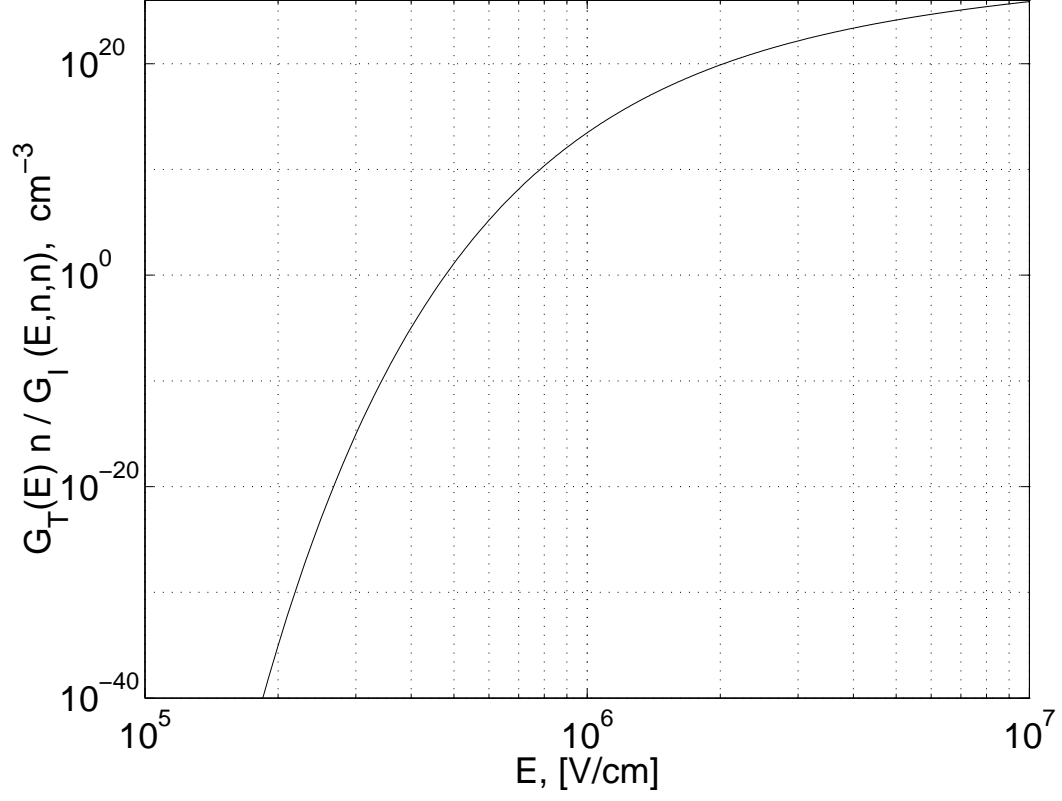


FIG. 4. Shown is the carrier concentration $n(E)$ for which impact ionization and tunneling ionization are of equal strength. This concentration can be expressed as the ratio $G_T(E)n/G_I(E,n,n)$, where we assumed $n = p$ and neglected the cut-offs in (9).

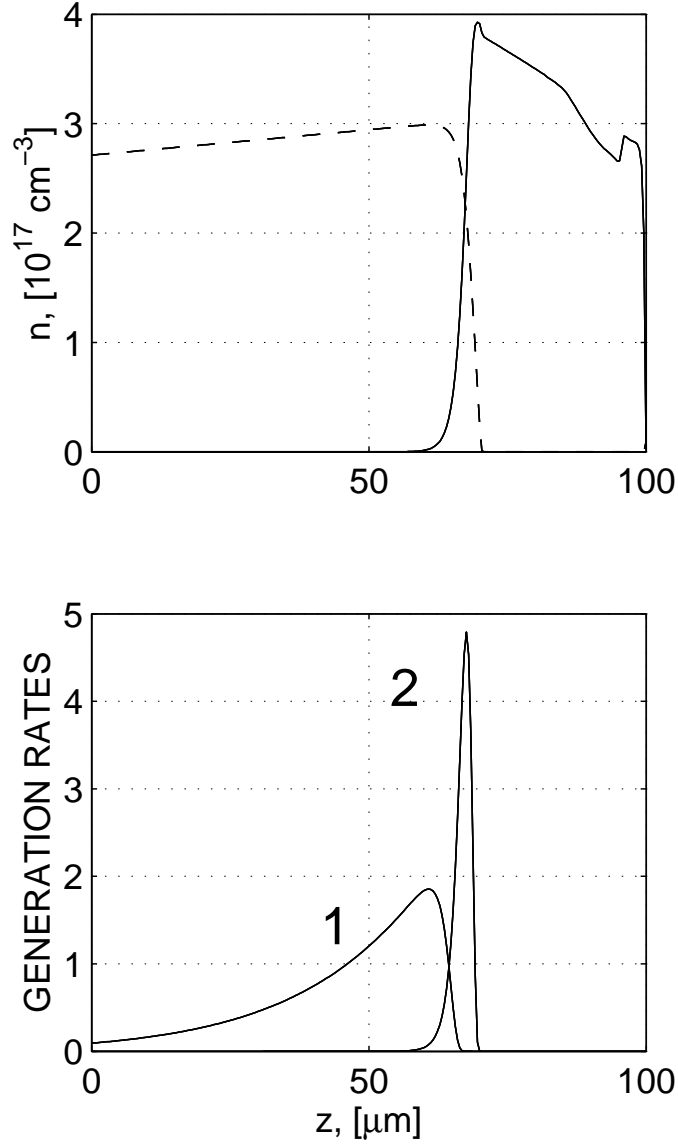


FIG. 5. The inner structure of the tunneling-assisted front at some instant of time ($t = 740$ ps). The upper panel shows the electron concentration (solid line) and the electrical field profile (dashed line, in arbitrary units). The lower panel shows spatial profiles of the tunneling generation rate G_T (curve 1, one unit corresponds to $10^{27}/\text{s} \cdot \text{cm}^3$) and the impact ionization rate G_I (curve 2, one unit corresponds to $10^{36}/\text{s} \cdot \text{cm}^3$). Note the different scales of G_T and G_I .

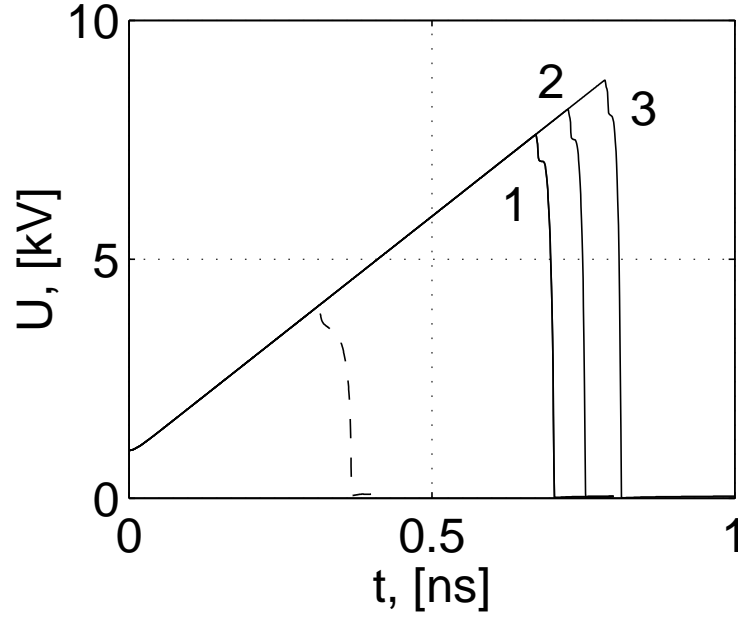


FIG. 6. Voltage at the device $U(t)$ calculated for different cut-offs $n_{cut} = p_{cut} = 10^8$, 10^9 , $5 \cdot 10^9 \text{ cm}^{-3}$ (curves 1,2,3, respectively). The dotted line shows the unphysical premature switching in a low electrical field obtained for $n_{cut} = p_{cut} = 0$.